

Analysis and Design of Photobioreactors for Microalgae Production II: Experimental Validation of a Radiation Field Simulator Based on a Monte Carlo Algorithm

Josué Miguel Heinrich^{1,2}, Ignacio Niizawa¹, Fausto Adrián Botta^{1,2}, Alejandro Raúl Trombert² and Horacio Antonio Irazoqui^{*1,2}

¹Group of Innovation on Bio-processes Engineering, Institute for the Technological Development of the Chemical Industry (INTEC), National Research Council (CONICET) and University of Litoral (UNL), Santa Fe, Argentina

²Group of Innovation on Bio-processes Engineering, Department of Biochemistry and Biological Sciences (FBCB), University of Litoral (UNL), Ciudad Universitaria, Santa Fe, Argentina

Received 20 December 2011, accepted: 14 March 2012, DOI: 10.1111/j.1751-1097.2012.01149.x

ABSTRACT

2 In previous study, we developed a methodology to assess the intrinsic optical properties governing the radiation field in algae suspensions. With these properties at our disposal, a Monte Carlo simulation program is developed and used in this study as a predictive autonomous program applied to the simulation of experiments that reproduce the common illumination conditions that are found in processes of large scale production of microalgae, especially when using open ponds such as raceway ponds. The simulation module is validated by comparing the results of experimental measurements made on artificially illuminated algal suspension with those predicted by the Monte Carlo program. This experiment deals with a situation, which resembles that of an open pond or that of a raceway pond, except for the fact that for convenience, the experimental arrangement appears as if those reactors were turned upside down. It serves the purpose of assessing as to what extent the scattering phenomena are important for the prediction of the spatial distribution of the radiant energy density. The simulation module developed can be applied to compute the local energy density inside photobioreactors with the goal to optimize its design and their operating conditions.

INTRODUCTION

Microalgae are microscopic algae typically found in freshwater and marine environments (1). In recent years, they have drawn much attention because of their capability of producing large amounts of lipids, which can be used as raw material in biodiesel production (2). Like terrestrial plants, algae obtain from light the energy needed for growth and to perform the rest of the cellular functions. When compared with terrestrial crops, microalgae production for the biofuels industry presents several advantages (3–5): they can grow almost anywhere, requiring just sunlight and some simple nutrients; different

microalgae species can be adapted to live in a variety of environmental conditions; they have much higher growth rates and productivity; they are easy to cultivate; they have the possibility of using water unsuitable for human consumption and can be grown in infertile areas.

Microalgae mass production is carried out either in open ponds or closed photobioreactors (PBRs; 6). Open ponds are easier to construct and operate than most PBRs, but their use brings about a poor utilization of light, as well as evaporative losses, transfer of CO₂ to the atmosphere, and the need for large areas exposed to sunlight (7–9). A more serious difficulty of open systems is the high risk of contamination with other microalgae species and other organisms. Closed PBRs show several advantages over open ponds: they allow a better control of the culture conditions (such as temperature, pH, degree of mixing, CO₂ and O₂ concentrations), prevent evaporation and also reduce CO₂ losses to the environment; contamination risks are lower, and allow attaining higher microalgae concentrations and volumetric productivities (10). Differences between PBRs for microalgae cultivation include variations in: size and shape of the reactor, construction materials, stirring and aeration systems, etc. These features have an impact not only on the reactor cost and its durability, but also on the way that light is distributed inside the algal suspension, which ultimately determines the performance and productivity of the reactor. The PBRs productivity is largely determined by the microalgae growth rate, which depends on the local radiant energy density profile in the reactor and on the programmed illumination strategy of the culture (11).

Therefore, to meet pre-established criteria of optimal design or optimal operation of PBRs, a physical and mathematical model must be developed including the characteristics of each proposed device. This model should be the base of a computer software with the possibility of being operated either in simulation mode to identify the optimal set of values of the operating variables for a given PBR, or in design mode to choose the optimal configuration of the PBR for a given set of operating variables. A precise mathematical model must take into account and accurately reproduce all the relevant variables acting in the system (12). A fundamental part of this simulation program

*Corresponding author email: hirazo@santafe-conicet.gov.ar (Horacio Antonio Irazoqui)

© 2012 Wiley Periodicals, Inc.

Photochemistry and Photobiology © 2012 The American Society of Photobiology 0031-8655/12

1 must be based on physical and mathematical models of the
 2 properties of the radiation field needed for the prediction of the
 3 local monochromatic energy density. Low values of local energy
 4 density can limit the algae growth rate and high values can
 5 saturate the local rate of radiant energy absorption useful for
 6 growth, thus reducing the bioreactor energy efficiency (13,14).
 7 The simulation of the radiation field in algae cultures requires
 8 knowing the absorption coefficient of the suspension as a
 9 function of the absorbing pigment concentrations, as well as the
 10 scattering coefficient depending on the total biomass concen-
 11 **3** tration expressed as dry matter (15; Table 1).

12 In this study, a stochastic algorithm, based on the Monte
 13 Carlo method (16), is used to simulate the radiation field in an
 14 algal suspension and the physical and algorithmic basis were
 15 presented in detail in an earlier study (15). To validate exper-
 16 imentally the program based on the Monte Carlo algorithm as a
 17 simulation tool, a previously *ad hoc* constructed device (17) is
 18 utilized in this study. Three sets of experiments were performed
 19 in this study, using algae suspensions of different concentrations
 20 in each of them. The results of each run were compared with the
 21 values predicted by a Monte Carlo simulation program appropri-
 22 ate for the experimental setup used.

23 This experiment deals with a situation, which resembles that
 24 of open ponds such as raceway ponds, except for the fact that,
 25 for convenience, the experimental arrangement appears as if
 26 those reactors were turned upside down. It serves the purpose
 27 of assessing as to what extent the scattering phenomena are
 28 important for the prediction of the spatial distribution of the
 29 radiant energy density, and it also offers a reference for
 30 establishing the accuracy of simplified models. The simulation
 31 module developed can be applied to compute the local energy
 32 density inside a PBR with the goal to optimize its design or
 33 their operating conditions, thus achieving a more efficient
 34 production system.

35 MATERIALS AND METHODS

36 *Preparation of algal suspensions: algal strain and culture medium.* A
 37 strain of *Chlorella* sp. (kindly provided by Dr. A.M. Gagneten,
 38 FHUC, UNL) was used as model microorganism. Volumes of 750 mL
 39 of BG-11 (18) culture medium were sterilized in sealed Erlenmeyer
 40 flasks and inoculated with the isolated species of alga. The batch
 41 culture was axenically grown by exposing it to artificial light provided
 42 by a daylight lamp Philips 15 W. The suspension was well mixed by
 43 a bubbling atmospheric air stream, previously sterilized by flowing it
 44 through a 0.45 μm pore size filter. The atmospheric air stream supplies
 45 the CO_2 that is necessary for the culture growth, and at the same time,
 46 strips off the O_2 generated by oxygenic photosynthesis. The operation
 47 was continued until a sufficiently high-biomass concentration was
 48 reached (typically between 1.0 and 2.0 g DW L^{-1}).

49 *Measurement of biomass concentration in algal cultures.* The mass
 50 concentration of algae in the batch cultures was determined by
 51 measuring the dry weight (DW) of the total suspended solids (TSS; 19)
 52 contained in an aliquot of each suspension. The algal mass contained in a
 53 50 mL sample was collected on a filter of 0.45 μm pore diameter; then it
 54 was washed with 30 mL of distilled water and dried at 100°C during

55 **Table 1.** Results of biomass concentration and chlorophyll content of
 56 reference suspensions of *Chlorella* sp.

57 Concentration in reference suspension	<i>Chlorella</i> sp.
58 Biomass [g DW L^{-1}]	1.42
59 Chlorophylls [mg g^{-1} DW]	47.4

60 DW, measurement of biomass dry weight.

60 min. The DW of the solids originally suspended in the processed
 sample, representative of the whole culture, was computed as the
 difference between the DW of the clean filter and that of the filter with
 the retained solids. The mass concentration of algae is expressed as the
 DW of suspended solids per unit volume of the sample, which in turn is
 the DW of suspended solids per unit volume of the culture. Finally, from
 aliquots of the culture suspension, samples of one tenth and one
 hundredth the concentration of the original culture were prepared.

Measurement of the specific chlorophyll content in the culture media. The total chlorophyll content in the culture media was determined
 by the method reported by Ritchie (20). Aliquots of the cultures were
 centrifuged to collect the suspended cells. The cells were washed with
 distilled water and then they were centrifuged again. The harvested cells
 were suspended in methyl alcohol and the chlorophylls were extracted
 by heating the methyl suspension at 80°C during 5 min. The chlorophylls
 content of the algal suspensions was calculated using the measured
 values of absorbance at three different wavelengths (632, 652 and
 665 nm), as well as the absorbance coefficients reported in the quoted
 paper, and it was expressed as mg of chlorophylls per g DW of microalgae.

Physical and mathematical model of light transfer. Light transfer
 within an absorbing and scattering medium, such as a PBR, is
 governed by the radiative transport equation (RTE), which is an
 integral-differential equation that can be written in terms of the
 spectral intensity. Several models for the calculation of the distribu-
 tion of light in PBRs have been reported in the literature (13,21–24).
 In a recent review, Pilon *et al.* (25) presented different solutions of the
 RTE inside PBRs: (1) Beer–Lambert’s law, which provides the
 solution of the one-dimensional steady-state RTE accounting for both
 absorption and out-scattering but disregarding in-scattering; (2) two-
 flux approximation; and (3) discrete ordinate methods. Another
 possibility is the physical simulation of the radiation avoiding the
 inherent difficulties in solving the RTE. In this study, a stochastic
 algorithm, based on the Monte Carlo method (16), is used to simulate
 the radiation field in an algal suspension. This method emulates
 physical reality by tracking photons along their paths through an
 algal suspension to eventually reach its boundaries. The advantage of
 such method relies on the fact that it enables to handle the optical
 phenomena occurring within the suspensions and on their boundaries,
 with the characteristics of the light emitted by radiant energy sources
 without the need of introducing simplifications to make the problem
 mathematically manageable.

As it was previously said, the basis of the Monte Carlo simulation
 of the radiation field in microalgae suspensions were presented in detail
 in an earlier study (15), where we have applied this method to assess
 the scattering volumetric coefficient ξ_i ; the absorption volumetric **4**
 coefficient α_i ; and the parameters of the scattering phase function
 $B(\mu_0)$, all of them in homogeneous algal suspensions. From the
 experimental results obtained, it was concluded that the scattering
 phase function can be modeled as independent of wavelength, and that
 the scattering coefficient can be correlated through a linear relation
 with the mass concentration of microalgae

$$\xi_i \left[\frac{1}{\text{mm}} \right] = \xi_i^{\text{sp}} \left[\frac{\text{L}}{\text{mgmm}} \right] x \left[\frac{\text{mg}}{\text{L}} \right] \quad (1)$$

On the other hand, the absorption coefficient, which was shown to
 be highly sensitive to wavelength, has been correlated with the
 chlorophyll concentration.

$$\alpha_i \left[\frac{1}{\text{mm}} \right] = \alpha_i^{\text{chl}} \left[\frac{\text{L}}{\text{mgmm}} \right] \text{Chl} \left[\frac{\text{mg}}{\text{L}} \right] \quad (2)$$

In doing this, the highest weights were assigned to the experimental
 values taken at wavelengths within the intervals where chlorophylls are
 the principal absorbent pigments. Experimental results also show that
 light in algae suspensions is scattered strongly in the forward
 directions, in agreement with abundant reported results (25–27). On
 the basis of this evidence, the scattering phase function $B(\mu_0)$ has been
 successfully approximated as a six-term, five-parameter expansion on
 Legendre polynomials

$$B(\mu_0) = 1 + \sum_{n=1}^5 c_n P_n(\mu_0) \quad (3)$$

For Monte Carlo simulation purposes, ξ_λ and α_λ for homogeneous algae suspensions were related to the cumulative probability of occurrence of absorption, $P(A)$,

$$P(A) = \frac{n_p^{(\text{abs})}(s + \Delta s, \hat{\Omega}, v)}{n_p(s, \hat{\Omega}, v)} = \frac{\alpha_v}{(\alpha_v + \xi_v)} \{1 - \exp[-(\alpha_v + \xi_v)\Delta s]\} \quad (4)$$

and of scattering of photons, $P(S)$,

$$P(S) = \frac{\xi_v}{(\alpha_v + \xi_v)} \{1 - \exp[-(\alpha_v + \xi_v)\Delta s]\} \quad (5)$$

while they travel a distance Δs through a homogeneous algal suspension.

The cumulative probability $P(\text{NA}, \text{NS})$ that photons travel a distance Δs in the direction $\hat{\Omega}$ without being absorbed nor scattered, is

$$P(\text{NA}, \text{NS}) = \exp\{-(\alpha_v + \xi_v)\Delta s\} \quad (6)$$

We have assumed that the motion of the photons in the radiation field obeys the laws of classical many-body systems except for the fact that they all move with the same speed, *i.e.* with the speed of light. With this picture in mind, we defined the photon number density function $n_p(\underline{r}, \hat{\Omega}, \lambda)$, that represents the number of photons around the position \underline{r} in the radiation field, which move in the direction $\hat{\Omega}$ and their wavelengths are within the range from λ to $\lambda + d\lambda$ (*i.e.* the number density of $(\underline{r}, \hat{\Omega}, \lambda)$ -photons, for short). With this definition, the contribution to the local radiant energy density of λ -photons about the position \underline{r} , $e(\underline{r}, \lambda)$, can be set as follows:

$$e(\underline{r}, \lambda) = h\lambda \int_{\hat{\Omega}} d^{(2)}\hat{\Omega} n_p(\underline{r}, \hat{\Omega}, \lambda) = h\lambda \int_0^{2\pi} d\phi \int_{-1}^1 d\mu n_p(\underline{r}, \mu, \phi, \lambda) \quad (7)$$

To validate experimentally the program based on the Monte Carlo algorithm as a simulation tool, a previously *ad hoc* constructed device (17) is utilized in this study. This device has a light source that illuminates indirectly the bottom a Petri dish with almost vertical rays reflected on a straight parabolic mirror. After leaving the suspension through its upper liquid-air interface with different directions, the energy of the scattered rays is recorded by a radiometer placed at different positions on a virtual cupola symmetrically covering the sample dish.

Through the suspension, the initially almost vertical beams can undergo two different phenomena: dispersion and absorption. The magnitudes of these effects are directly related with the algal mass concentration and to the chlorophyll content in the sample, respectively.

In parallel, a computational algorithm based on the Monte Carlo method was developed to simulate the radiation field in the experimental setup. In that algorithm, the fluorescent lamp was modeled as a superficial and isotropic cylindrical light emitter. Within the algal suspension, the photon scattering probability and that of photon absorption were computed by means of equations (4) and (5), using the correlation between ξ_λ and the algae DW concentration, and between α_λ and the chlorophylls concentration, respectively, obtained in previous study. Whenever a photon is deflected from its previous trajectory by a scattering event, a probability based on the phase function, satisfactorily approximated by an expansion on Legendre polynomials, is assigned to the new direction (15).

Three sets of experiments were performed in this study, using algae suspensions of different concentrations in each of them. The results of each run were compared with the values predicted by a Monte Carlo simulation program appropriate for the experimental setup used. The simulator was fed with the parameters ξ_λ , B and α_λ , which have been determined in a previous study through three independent experiments using different experimental devices in each of them, resulting from different arrangements of their component parts, *i.e.* the monochromatic light source, the radiant energy detector, the cuvette bearing the suspension sample and the integration sphere.

The simulation program is validated by comparing the energy fluxes predicted, with the experimental values of such fluxes which leave, in different directions, a Petri dish containing a suspension sample of different concentration for each experimental run, confirming at the same time the intrinsic character of the parameters ξ_λ , B and α_λ .

Experimental device for the measurement of directional fluxes of radiant energy. To check the accuracy of the developed model, the directional fluxes of radiant energy were measured with the same experimental setup used by Imoberdorf *et al.* (2007; 17), although for different purposes. It consists of two separate parts (Fig. 1): the radiation source (c) and the measurement device (d). The latter allows measuring the light irradiance at different polar θ_d and azimuthal ϕ_d angles. Between the light source and the detector, there is a Petri dish (a) containing the algal suspension. This Petri dish is 135 mm diameter with its cylindrical wall blackened. Its bottom was also blackened, except for an 88 mm diameter circle at its center, which remains transparent to visible light.

The radiation source consists of a daylight tubular fluorescent lamp (25 mm outer diameter and 15 W power output; b). The lamp axis is aligned with the focal line of the right parabolic mirror (f), thus providing nearly coplanar rays by reflection on the mirror. Direct irradiation from the lamp to the bottom of the Petri dish is avoided by placing a narrow black sheet, which absorbs the radiation from the lamp that otherwise would have reached the dish containing the algal suspension (g). To eliminate from the light source output those rays too tilted toward the direction of the lamp axis, they were absorbed on blackened thin fins (e), arranged perpendicularly to the lamp axis and at regular distances from one another. This screen was placed on top of the lamp-mirror radiation source. The fins are 70 mm height and are placed at 8.2 mm distance from each other.

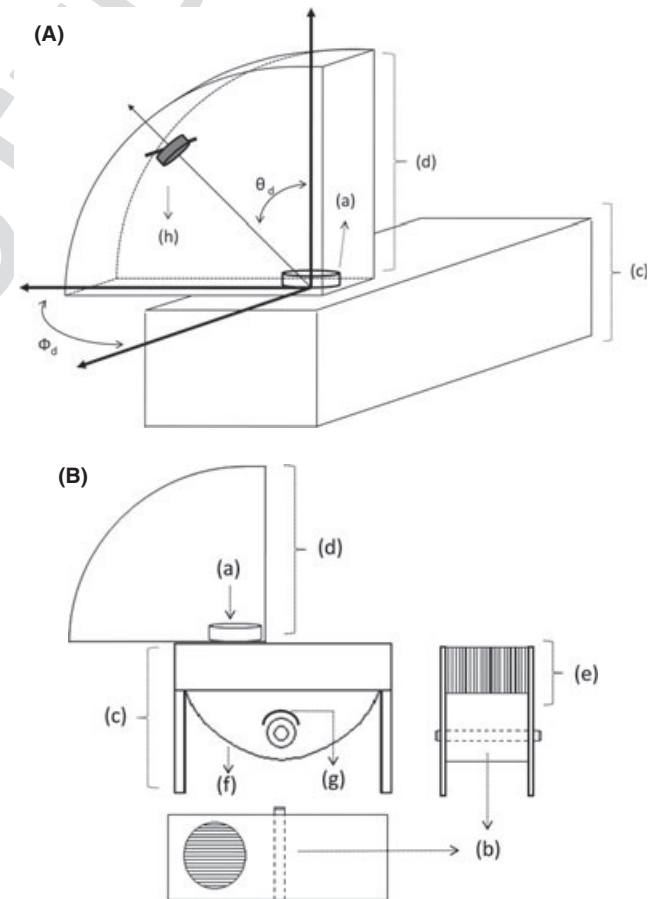


Figure 1. (A) Schematic representation of the *ad hoc* built device for directional fluxes of radiant energy measurements. (a) Petri dish, (b) daylight lamp, (c) emitting system, (d) measuring device, (e) screen of blackened plates, (f) parabolic mirror, (g) blackened cover. (B): Another schematic representation of the *ad hoc* built device for directional fluxes of radiant energy measurements. (a) Petri dish, (b) daylight lamp, (c) emitting system, (d) measuring device, (e) screen of blackened plates, (f) parabolic mirror, (g) blackened cover, (h) radiometer detector.

The measuring device (d) consists of a Vis-radiometer (International Light IL-1700 SED005/W) mounted on a support that allows changing the (θ_d, ϕ_d) position of the detector (h) while maintaining a constant distance of 350 mm from a mid-depth point in the algal suspension to the center of the Petri dish. The detection planar surface is always aimed at that central point.

The almost vertically collimated rays coming from the light-emitting setup, reaches into the algal suspension after being transmitted through the glass bottom of the dish. After undergoing absorption and scattering, they leave the suspension with different intensities, as well as with different directions. Directional radiation fluxes were measured at different polar angles, θ_d , and azimuthal angles, ϕ_d , in a series of five experiments, corresponding to three different algal concentrations, another for pure BG11 culture medium and the last one with the empty Petri dish. The readings were made with the radiometer placed at the following θ_d angles: 0, 5, 10, 15, 20, 25, 35 and 45°, and at the ϕ_d angles: 0, 10, 20, 30, 40 ... and 350°.

Simulation algorithm of the radiation model experimental test. As previously mentioned, the radiation source includes a daylight fluorescent lamp arranged coaxially with the focal line of a parabolic mirror. This device delivers almost parallel reflected rays. Their deviation from the vertical direction is due to the following reasons: (1) the isotropic superficial emission of the lamp within the hemisphere with the local normal vector oriented toward the outside of the lamp as its symmetry axis; and (2) the lamp has a non-negligible radius compared to the parabolic mirror size (Fig 2).

In a broad sense, the computational simulation of the experiments consists in firing a large number of photons from every point on the surface of the lamp, in uniformly distributed random directions within the hemisphere with the local normal vector oriented toward the outside of the lamp as its symmetry axis; and in tracking their paths to the positions in the suspension where they are absorbed, or to the points on the suspension-air interface where they left the sample. Although, the simulation algorithm computes the trajectory of the photons one by one in successive calculations, it must be remembered that they are all contemporary. The algorithm starts by generating a photon at a randomly chosen position over the lamp surface, with a random $\underline{\Omega}(\phi, \theta)$ initial direction. Considering the design of the *ad hoc* built setup, the photons emitted by the lamp have three possible targets: (1) one of the two blackened parabolic end walls, which serve as templates to shape the parabolic mirror made of a highly reflecting aluminum sheet; (2) the narrow black sheet positioned on top of the lamp, which absorbs the radiation that otherwise would directly reach the dish containing the algal suspension (3) the reflecting parabolic mirror. If one of the first two events occurs, the photon is absorbed and a new one has to be generated. If the photon hits the parabolic mirror, the algorithm computes the impact position and the reflection direction of the photon. It checks whether the photon flies all the way through the gap between two neighboring blackened fins, thus leaving the radiant energy source as part of an almost vertical ray, or it is absorbed by one of the fins in the screen on top of the radiation source. If the photon flies all the way through the gap, the algorithm checks whether it hits the transparent circle at the base of the Petri dish or not. If it does, it enters the algal suspension and describes a trajectory that results from the random events it can undergo.

Monte Carlo simulation in the algal suspension. The results obtained with the Monte Carlo simulation algorithm were compared with those from experimental measurements to test the model predictive capabilities. The experimental data consist in measurements of the irradiance in directions within the upper hemisphere centered at the Petri dish.

The algorithm is based on the assumption that each photon moves step-by-step through the suspension. In every stretch, the photon can be absorbed or scattered, or it can experiment a free flight without being absorbed nor deflected. One among these three events is selected by the generation of a random number as in a previous study (15). After every move of a photon, the algorithm checks whether it has hit a wall of the suspension container, the bottom of the dish, or if it has reached the suspension-air interface.

If a photon hits the black wall of the Petri dish, it is necessarily absorbed and removed from the radiative energy field. The bottom of the dish was modeled as a thin glass plate, with a circular central region transparent to radiation within the wavelength range of interest. The

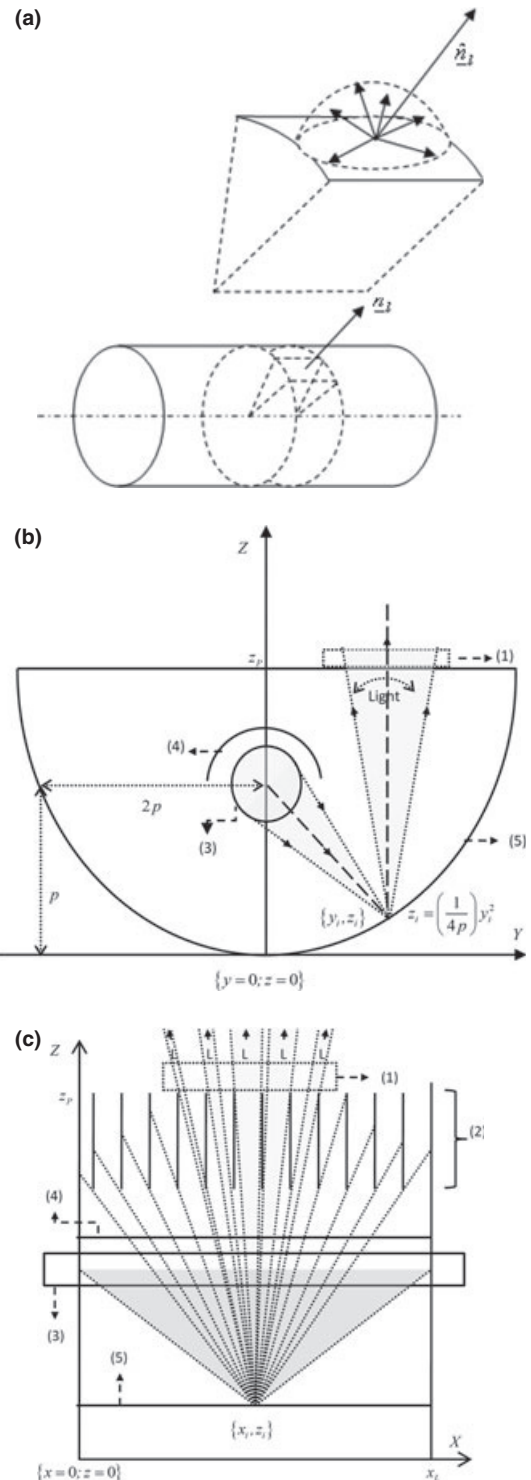


Figure 2. (a) Schematic representation of the isotropic superficial light emission of the fluorescent lamp. A surface element about the generic point i emits radiation isotropically within the hemisphere around the local normal \hat{n}_i . (b) Illustration of the deflection angles of reflected rays from the vertical plane, due to the finite radius of the lamp. Any $\{y_i, z_i\}$ point on the mirror receives light from all the surface of the lamp that is seen from that point. (c) Screening effect of the vertical blackened fins. Zones designated as L are the illuminated areas. (1) Petri dish, (2) screen of blackened vertical fins, (3) fluorescent lamp, (4) black sheet to avoid direct irradiation of the sample, (5) parabolic mirror, (p) parabolic focal distance (67.5 mm), (x_L) Width of the mirror (320 mm), (z_p) Height at which the bottom of the Petri dish is found (247 mm).

boundary between the algal suspension and air, on the other hand, was modeled as an interface that separates two fluid media of different optical properties. In the last two cases, the photon may be reflected back into the suspension, or it may be refracted into the neighboring phase. To tell which of these two complementary events occur, a new random number is generated, which is compared with the value of the reflectivity of the corresponding interface. This strategy has been presented with greater detail by Heinrich *et al.* (15). If a photon reaches the interface between the algal suspension and the air above, and it is not reflected, one more count should be added to the current number of photons of wavelength λ , refracted into the direction $\hat{\Omega}(\phi, \theta)$, provided that the new direction is enclosed by the solid angle with its apex at the center of the circular photon detector, and with its normal pointing at the center of the suspension–air interface, which is entirely included within the detector’s view angle.

To assess the probabilities of scattering and absorption, and to assign a new direction to the scattered photons, it is necessary knowing the scattering and absorption coefficients, and the coefficients of the phase function expansion on Legendre polynomials (15).

Directional measurement of irradiance. Both the scattering coefficient and the absorption coefficient depend on wavelength (23,27). The fluorescent lamp used in this experiment is far from being a monochromatic source, showing the emission spectrum presented in Fig. 3. Therefore, a procedure has to be devised to assign a wavelength to every photon emitted by the lamp.

In Fig. 3, the bars height representing the percentage of the output energy of the lamp emitted at different wavelengths was calculated as follows:

$$P_{\lambda}^{\%} = \frac{\int_{\lambda-\Delta\lambda/2}^{\lambda+\Delta\lambda/2} I_{\lambda'} d\lambda'}{\int_{400}^{700} I_{\lambda'} d\lambda'} \times 100 \quad (8)$$

Suppose, we choose a photon at random among those emitted from any elementary surface area on the lamp. Let us denote by $dG(\lambda)$ the differential probability that the photon had frequency between λ and $\lambda + d\lambda$. We can write

$$dG(\lambda) = n_p^L(\lambda) d\lambda \quad (9)$$

where

$$n_p^L(\lambda) = \frac{dG(\lambda)}{d\lambda} \quad (10)$$

is the probability distribution function that a photon fired from the lamp has frequency λ . The differential probability $dG(\lambda)$ can be interpreted as the fraction of photons with frequency within λ and $\lambda + d\lambda$ among the total set of emitted photons. Moreover, $n_p^L(\lambda)$ can be related to the light intensity as follows:

$$I_L(\lambda) = c h \left(\frac{c}{\lambda}\right) n_p^L(\lambda) \quad (11)$$

The expression of $dG(\lambda)$ is

$$dG(\lambda) = \left(\frac{\lambda}{hc^2}\right) I_L(\lambda) d\lambda \quad (12)$$

As we are only interested in the visible region of the electromagnetic spectrum, which is entirely included in the interval $400 \leq \lambda \leq 700$ nm, the following normalization condition was imposed on $G(\lambda)$

$$\tilde{G}(\lambda) = \left(\frac{1}{\kappa hc^2}\right) \int_{400}^{\lambda} I_L(\lambda') \lambda' d\lambda'; \quad (13)$$

$$400 \text{ nm} < \lambda < 700 \text{ nm}$$

where

$$\kappa = G(700 \text{ nm}) - G(400 \text{ nm}) = \left(\frac{1}{hc^2}\right) \int_{400}^{700} I_L(\lambda) \lambda d\lambda \quad (14)$$

and $\tilde{G}(\lambda) = [G(\lambda) - G(400 \text{ nm})] / \kappa$.

To assign a wavelength to each photon emitted from the lamp, a random number δ_{λ} is generated and λ is given by

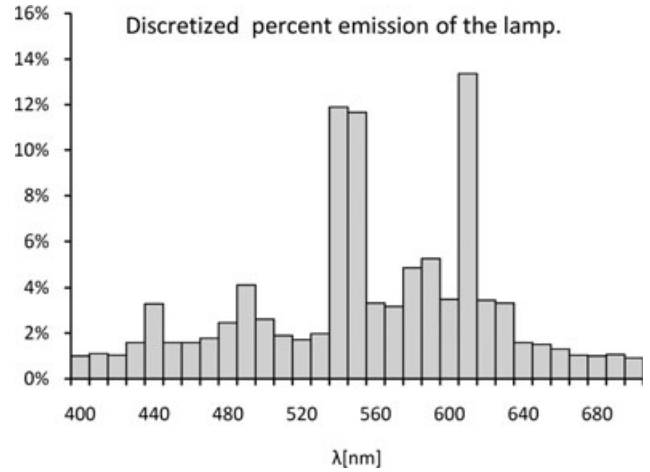


Figure 3. Discretized percent emission of the lamp vs wavelength (nm) within the visible region of the electromagnetic spectrum (based on the information contained in the product datasheet).

$$\delta_{\lambda} = \tilde{G}(\lambda) = \left(\frac{1}{\kappa hc^2}\right) \int_{400}^{\lambda} I_L(\lambda') \lambda' d\lambda'; \quad (15)$$

$$400 \text{ nm} < \lambda < 700 \text{ nm}; \quad 0 < \delta_{\lambda} < 1$$

Beams of photons leave the suspension through the upper liquid–air interface with different directions and carrying the residual energy after its depletion by absorption. The energy of the scattered rays is recorded by a radiometer placed at different (θ_d, ϕ_d) positions. The monochromatic radiant energy due to contribution of the $(\hat{\Omega}, \lambda)$ -photons hitting the detector surface ΔA per unit time and unit area is:

$$\frac{\Delta Q(\lambda, \phi_d, \theta_d)}{\Delta A \Delta t} = ch \left(\frac{c}{\lambda}\right) n_p^D(\lambda, \phi_d, \theta_d) \Delta \lambda \Delta \hat{\Omega} \cos \theta^D \quad (16)$$

where h is the Planck constant. The local irradiance $E_D(\phi_d, \theta_d)$ (W cm^{-2}) including all wavelengths and all incident directions at the (θ_d, ϕ_d) position is:

$$E_D(\phi_d, \theta_d) = \int_{\hat{\Omega}} \int_{\lambda} ch \left(\frac{c}{\lambda}\right) n_p^D(\lambda, \phi_d, \theta_d) d\lambda d\hat{\Omega} \cos \theta^D \quad (17)$$

Every photon captured by the detector produces a signal, which depends its wavelength through the detector’s relative responsivity $R(\lambda)$ (Fig. 4). The total output signal of the detector is the sum of the signals generated by each of the λ photons:

$$S(\phi, \theta) = \int_{\hat{\Omega}} \int_{\lambda} ch \left(\frac{c}{\lambda}\right) n_p^D(\lambda, \phi_d, \theta_d) R(\lambda) d\lambda d\hat{\Omega} \cos \theta^D \quad (18)$$

RESULTS AND DISCUSSION

“Angular Radiation Fluxes” experiment: validation of the Monte Carlo simulation algorithm

In previous study (28,29), Monte Carlo simulation was employed for light distribution calculation in a laboratory scale, perfectly mixed stirred tank reactor, for studying microalgal kinetics for modeling purposes. The authors did not calculate the intrinsic values of the parameters ξ_{λ} , B and α_{λ} , thus hindering the possibility of performing a systematic scale up.

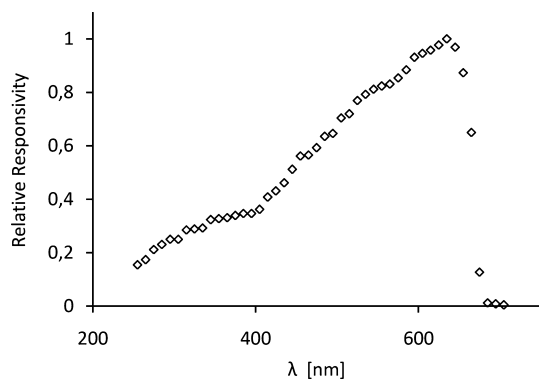


Figure 4. Relative responsivity $R(\lambda)$ of the detector. $R(\lambda)$ shows the variations of signal produced by photons reaching the detector according with the photon wavelength (nm). Adapted from the product datasheet.

The Monte Carlo simulation method is validated by comparing the predicted values of the directional fluxes of energy with their experimental values. These fluxes are due to photons that cross the suspension–air interface of each sample in different directions. Experiments were carried out for different concentrations of microalgae.

At the same time, these experimental runs offer a confirmation that the parameters ξ_λ , B and α_λ are independent of any particular feature of the experimental setup used to measure them in a previous study (15); *i.e.* that they are intrinsic parameters depending exclusively on the properties of the algal suspensions, such as their algal DW concentration and the chlorophylls concentration.

Regarding the radiative energy field, this experiment approximates what happens in open ponds such as raceway ponds. It serves the purpose of assessing as to what extent the scattering phenomenon is important for the prediction of the spatial distribution of the radiant energy density. The simulation module developed can be applied to compute the local energy density inside a PBR with the purpose of optimizing its design or their operating conditions, thus achieving a more efficient production system.

The experiments consist in the irradiation, from below, of a Petri dish containing different algal suspensions and in measuring the directional irradiance (W m^{-2}) at different positions over the upper hemisphere covering the suspension. The changes observed in the directional irradiances for different concentrations of algae are due to the combined effects of light absorption and scattering, with different prevalence of one over the other according to the suspension assayed.

The first step consists in modeling the *ad hoc* built light-emitting system. For simulation purposes, the lamp is modeled as a cylindrical surface, emitting isotropically from every surface element. The photon trajectories were simulated, and the predicted responses of the measurement device were compared with the data obtained experimentally.

The irradiances predicted by simulation for the case of the empty Petri dish, and those measured for the same conditions at different (θ_d, ϕ_d) positions of the detector, are plotted in Fig. 5 in two different formats. In Fig. 5a, experimental and simulated irradiances are plotted in polar coordinates as

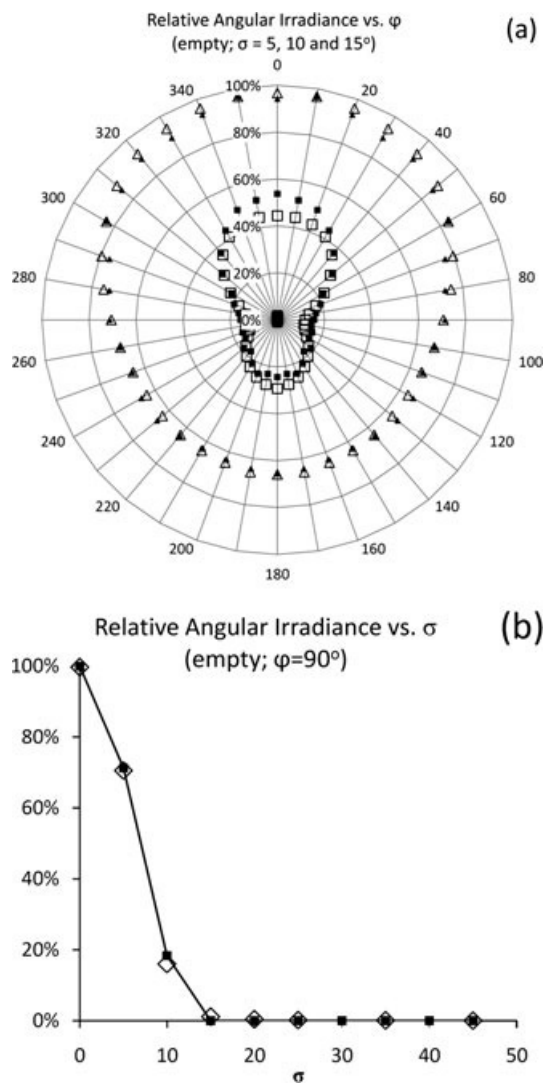


Figure 5. Directional irradiance for the case of the empty Petri dish, relative to the value at $\{\theta = 0^\circ; \phi = 90^\circ\}$ radiometer position. (a) Light irradiance against the azimuthal angle in polar coordinates for three different polar angles $\theta = 5^\circ$ (\triangle), 10° (\square) and 15° (\circ). Empty dots: experimental data, filled dots: model results. (b) Light irradiance against the polar angle (θ) for a constant azimuthal angle ($\phi = 90^\circ$). Empty dots: experimental data, line-filled dots: model results.

functions of the azimuthal angle (ϕ_d) for three polar angles ($\theta_d = 5, 10$ and 15°), whereas in Fig. 5b, measured and simulated irradiances are represented as functions of the polar angle (θ_d), for a single azimuthal angle (ϕ_d). As it can be seen in that figure, the simulation of the light-emitting device accurately reproduces the values of directional radiant energy fluxes measured with the aid of the radiometer (for angle definitions see Fig. 1).

Once the simulation module of the light-emitting device has been validated, we can do so with the Monte Carlo simulation method of a radiation field in an algal suspension. A Petri dish with an algal suspension is placed between the light-emitting system and the measurement device. The light irradiance on the detector will change depending on the combined effect of light absorption and scattering, with different prevalence of one over the other depending on the

suspension concentration. Using the coefficients of scattering and absorption and the scattering phase function from a previous study (15), the predicted values of the directional fluxes of radiant energy were compared with those experimentally obtained. In Fig. 6, measured and simulated radiant energy fluxes are plotted against the azimuthal angle, in polar coordinates, for three different polar angles and two different algal mass concentrations (Fig. 6a,b); all values are relative to the value at zero polar angle with the empty Petri dish. In Fig. 6a, it is shown how the light irradiance varies with the azimuthal angle for a 15 mg DW L⁻¹ algal suspension. Experimental values are compared with predicted ones at $\theta = 5, 10$ and 15° . From these results, it can be concluded that for this concentration (or for lower ones), experimental and predicted values of the radiant energy flux can be considered zero at polar angles larger than 15° , for all practical purposes. This effect is better illustrated in Fig. 7a. In Fig. 6b, the light radiation fluxes are shown at $\theta = 15, 35$ and 45° for a 1420 mg DW L⁻¹ algal suspension. Their magnitudes are similar, which can also be seen in Fig. 7c. The combined effect of light absorption, together with in-scattering and out-scattering, can be appreciated by comparing Fig. 6a with b: light irradiance strongly decreases with increasing θ at small polar angles, because light absorption and out-scattering are the dominant phenomena; but for larger angles the irradiance, initially zero, increases because of the in-scattering effect.

Figure 7a,b and c show how the radiant energy flux changes with the polar angle, for three different algal mass concentrations, and for a fixed azimuthal angle ($\phi = 90^\circ$). By comparing these three graphs, with that of Fig. 5a, which corresponds to the Petri dish filled with water, it can be observed that the trend followed by the combined effect of absorption and scattering phenomena when algal concentration increases. In the case of much diluted algal suspensions, the deviation of the light beams because of the presence of suspended cells is not significant; we can draw this conclusion by comparing Fig. 5b with Fig. 7a. In both cases, the shapes of the directional radiant energy flux profiles are very similar. The main difference between Figs. 5b and 7a is due to the attenuation of the radiant flux in the vertical direction, whereas the contribution of radiation to other directions as a consequence of light scattering is not a significant effect. In the case of more concentrated suspensions, like those corresponding to Figs. 7b and c, the in-scattering contribution to directions away from the vertical is an important effect, and the shape of the curves becomes more even, due to the larger attenuation as the consequence of the combined effect of light absorption and scattering in the vertical direction and the increased intensity due to scattering in other directions.

In Fig. 8, the effect of increasing the algal mass concentration at different directions results more apparent. In this figure, light intensity is plotted vs algal mass concentration at different polar angles for a fixed ($\phi = 90^\circ$) azimuthal angle. In the case of the more vertical directions, *i.e.* those for $\theta = 0, 5$ and 10° (Fig. 8a), the intensity of light decreases with increasing concentration of algae. This indicates that light absorption and out-scattering are the dominant effects. In directions farther from the vertical, *i.e.* $\theta = 25$ and 45° , initially an increase of the algal concentration results in a correlative

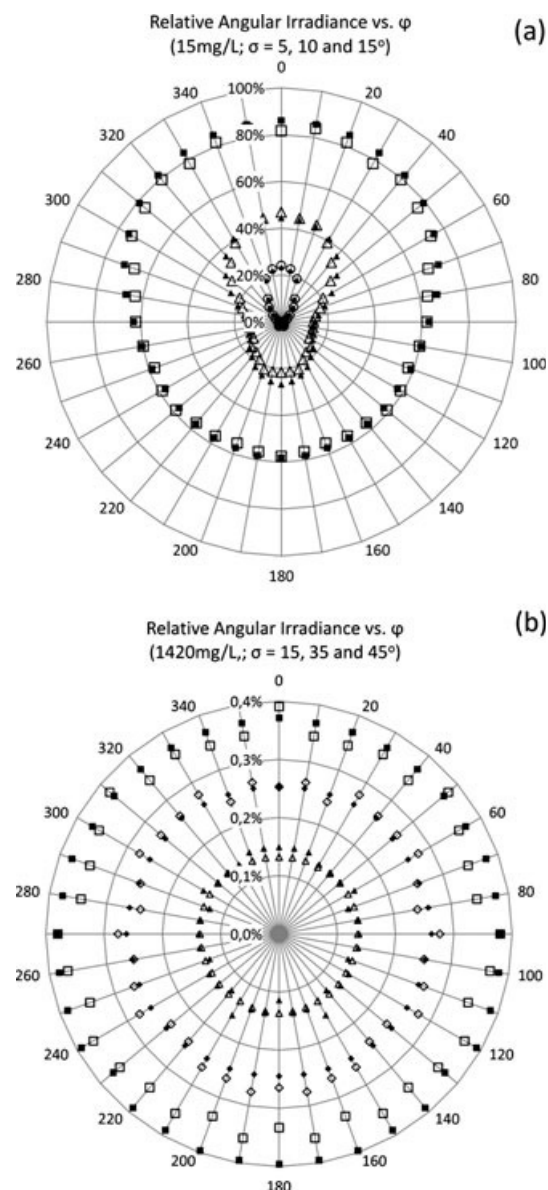


Figure 6. Light irradiance variation against the azimuthal angle for different polar angles, in polar coordinates. (a) Values corresponding to the 15 mg L⁻¹ microalgae suspension, at $\theta = 5(\Delta)$, $10(\square)$ and 15° (\circ). (b) Values for the 1420 mg L⁻¹ microalgae suspension, at $\theta = 5(\square)$, $10(\diamond)$ and 15° (Δ). Values are expressed as relative values referred to the measure at $\{\theta = 0^\circ; \phi = 90^\circ\}$ for the empty Petri dish. Empty dots: experimental data, line-filled dots: model results.

intensity increase, which is due to the relative prevalence of in-scattering over absorption. When the algal mass concentration becomes higher, light attenuation overrides this effect and light intensity tends to zero (Fig. 8b). As it can be seen in Figs. 6, 7 and 8, simulated angular radiation fluxes reproduce experimental values satisfactorily.

CONCLUSIONS

The results obtained with the Monte Carlo simulation algorithm were compared with experimental data to test the model predictive capabilities. Several conclusions can be drawn from

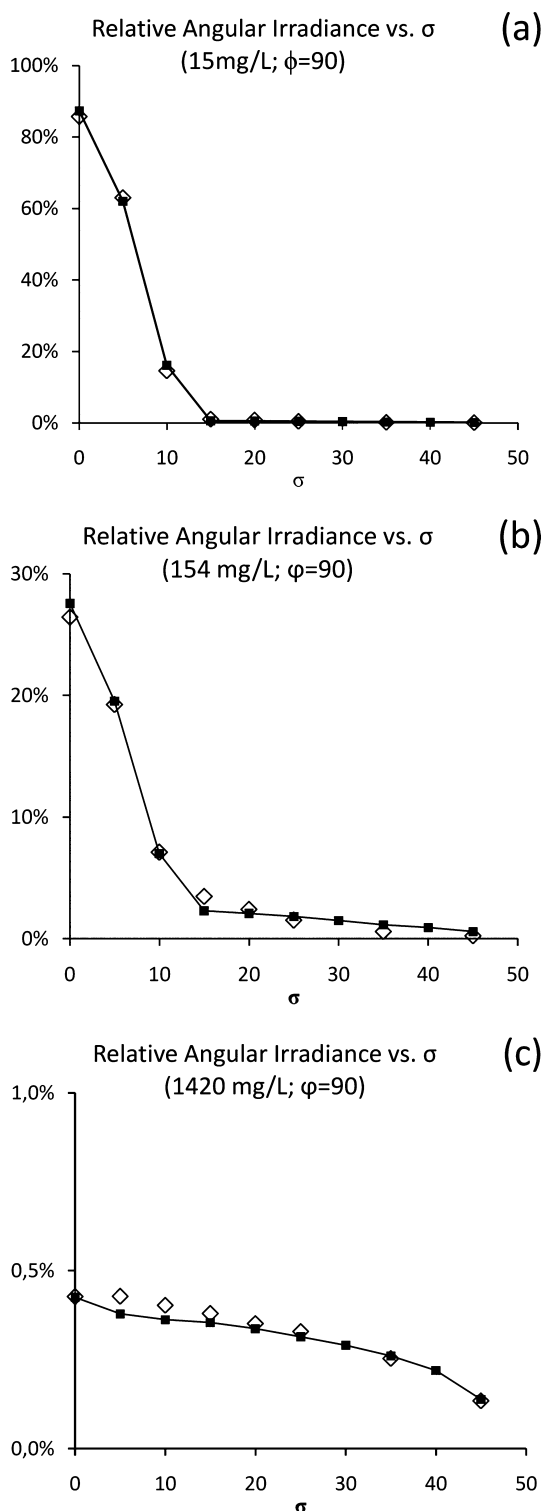


Figure 7. Irradiance dependence on the polar angle for different algal mass concentrations. The azimuthal angle remains unchanged ($\phi = 90^\circ$). (a) 15 mg L⁻¹, (b) 154 mg L⁻¹ y and (c) 1420 mg L⁻¹. Values are expressed as relative values referred to the measure at $\{\theta = 0^\circ; \phi = 90^\circ\}$ for the empty Petri dish. Empty dots: experimental data, line-filled dots: model results.

this comparison: (1) The proposed model of algae suspensions, and the stochastic simulation algorithm based on that model, are able to reproduce those features of the interaction between

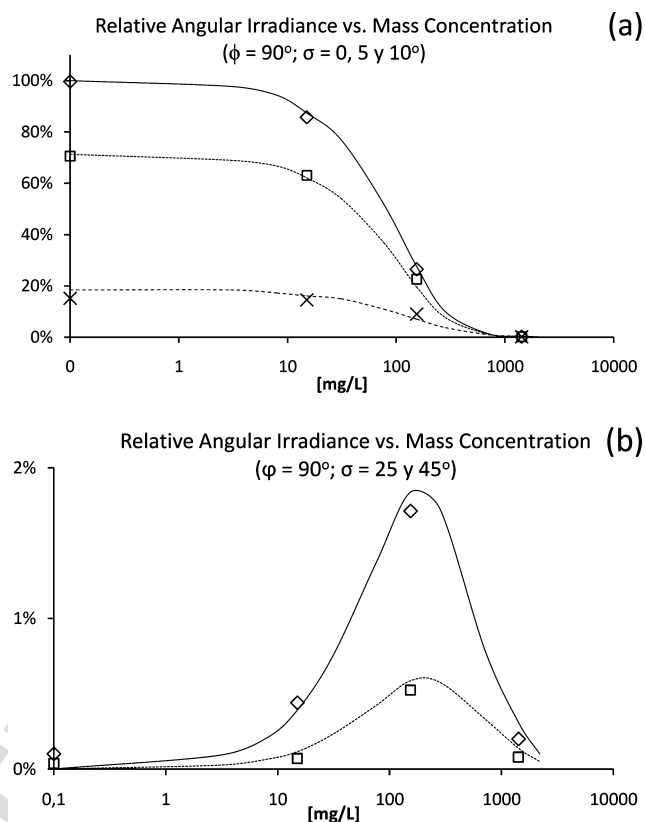


Figure 8. Irradiance variation against microalgal mass concentration for different polar angles and $\phi = 90^\circ$. (a) Values for $\theta = 0^\circ$ (\diamond , —), 5° (\square , ...) and 10° (\times , - -). (b) Values for $\theta = 25^\circ$ (\diamond , —) and 45° (\square , ...). Values are relative to the reference value in the $\{\theta = 0^\circ; \phi = 90^\circ\}$ direction, with the Petri dish empty. Dots: experimental data, lines: model results.

the radiation field and the algal suspension through which the field propagates, that are of interest for the design and optimization of PBRs; (2) The optical parameters obtained in an earlier study reproduce with accuracy the optical phenomena experienced by light beams traveling through microalgae suspensions of different concentrations, independently of the configuration features of the setup including the radiative energy source and the culture vase (*i.e.* they are intrinsic parameters); and (3) The scattering of light in algal suspensions is a significant phenomenon to take into account when the algal mass concentration exceeds a threshold value of around 100 mg DW L⁻¹.

The availability of this simulation algorithm makes it possible the prediction of the spectral photon density at any point within an algal culture and, consequently, of the local volumetric rate of photon absorption. As it is widely known, the latter is a property of the radiative field closely related to the local rate of microalgae growth.

Acknowledgements—This work has been supported by Universidad Nacional del Litoral, CAI + D Redes N°9 “Reactores y Procesos Biológicos para la Producción de Microorganismos Sustitutos de Agroquímicos y para la Obtención de Materias Primas Alternativas para la Fabricación de Biocombustibles” and by Consejo Nacional de Investigaciones Científicas y Técnicas de la República Argentina (CONICET) PIP IU “Modelado y optimización de foto-bio-reactores

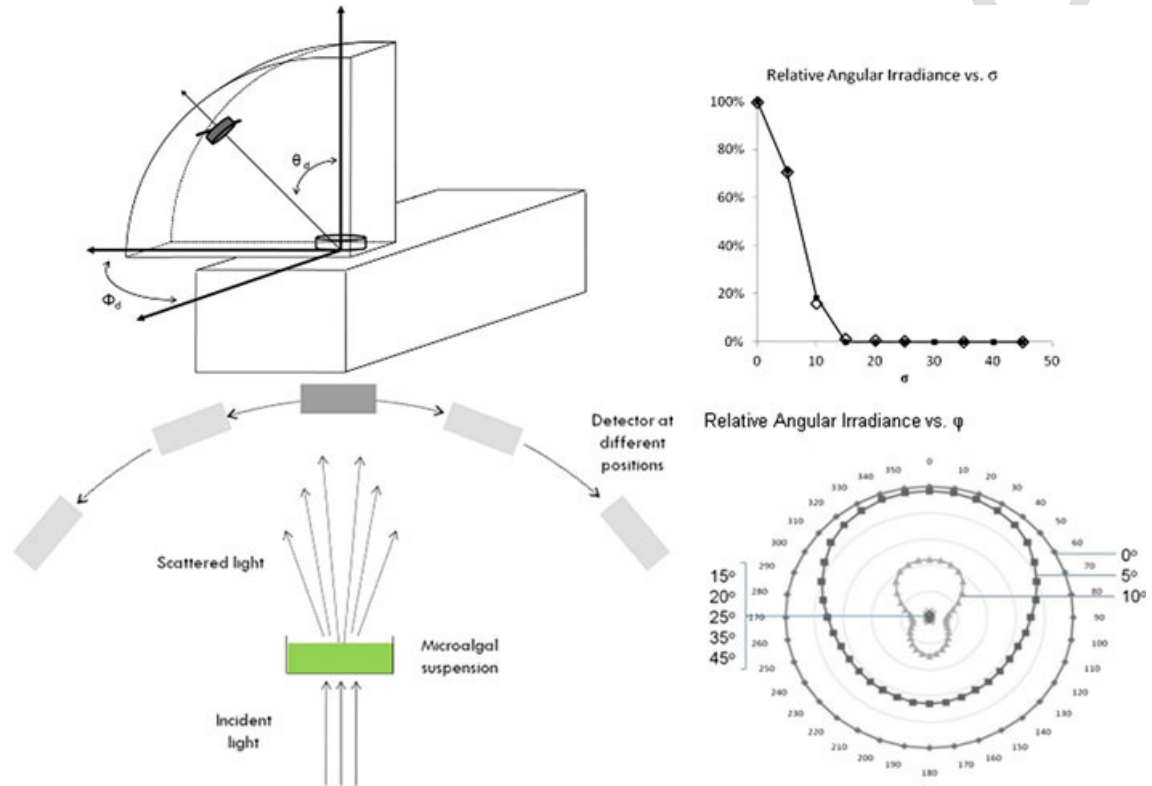
destinados al cultivo de microorganismos fototróficos para diferentes aplicaciones biotecnológicas". The authors are grateful to Emilio Saita for his generous contribution in part of the experimental work and to Mr. Ramón A. Saavedra and Mr. Antonio Negro for the technical support provided.

REFERENCES

1. Thurman, H. V. (1997) *Introductory Oceanography*, pp. ???–???. Prentice Hall College, NJ.
2. Hu, Q., M. Sommerfeld, M. Posewitz, M. Seibert and A. Darzins (2008) Microalgal triacylglycerols as feedstocks for biofuel production: perspectives and advances. *Plant J.* **54**, 621–639.
3. Mata, T. M. (2010) Microalgae for biodiesel production and other applications: a review. *Renew. Sust. Energ. Rev.* **14**, 217–232.
4. Li, Y., M. Horsman, N. Wu, C. Q. Lan and N. Dubois-Calero (2008) Biofuels from microalgae. *Biotechnol. Prog.* **24**(4), 815–820.
5. Chisti, Y. (2007) Biodiesel from microalgae. *Biotechnol. Adv.* **25**(3), 294–306.
6. Eriksen, N. T. (2008) The technology of microalgal culturing. *Biotechnol. Lett.* **30**(9), 1525–1536.
7. Boussiba, S., E. Sandbank, G. Shelef, Z. Cohen, A. Vonshak, A. Ben-Amotz, S. Arad and A. Richmond (1988) Outdoor cultivation of the marine microalga *Isochrysis galbana* in open reactors. *Aquaculture* **72**, 247–253.
8. Tredici, M. R. and R. Materassi (1993) From open ponds to vertical alveolar panels: the Italian experience in the development of reactors for the mass cultivation of photoautotrophic microorganisms. *J. Appl. Phycol.* **4**, 221–231.
9. Hase, R., H. Oikawa, C. Sasao, M. Morita and Y. Watanabe (2000) Photosynthetic production of microalgal biomass in a raceway system under greenhouse conditions in Sendai City. *J. Biosci. Bioeng.* **89**, 157–163.
10. Ugwu, C. U., H. Aoyagi and H. Uchiyama (2008) Photobioreactors for mass cultivation of algae. Review. *Bioresource Technol.* **99**, 4021–4028.
11. Molina Grima, E., F. G. Acien Fernández, F. García Camacho and Y. Chisti (1999) Photobioreactors: light regime, mass transfer, and scaleup. *J. Biotechnol.* **70**, 231–247.
12. Cassano, A. E., C. A. Martin, R. J. Brandi and O. M. Alfano (1996) Photoreactor analysis and design: fundamentals and applications. *Ind. Eng. Chem. Res.* **34**, 2155–2201.
13. Cornet, J. F., C. G. Dussap and G. Dubertret (1992) Structured model for simulation of cultures of the cyanobacterium *Spirulina platensis* in photobioreactors: I. Coupling between light intensity transfer and growth kinetics. *Biotechnol. Bioeng.* **40**, 817–825.
14. Cornet, J. F., C. G. Dussap and J. B. Gros (1998) Kinetics and energetics of photosynthetic micro-organisms in photobioreactors: application to *Spirulina* growth. *Adv. Biochem. Eng./Biotechnol.* **59**, 153–224.
15. Heinrich, J. M., I. Niizawa, F. A. Botta, A. R. Trombert and H. A. Irazoqui (2012) Analysis and design of photobioreactors for microalgae production I: method and parameters for radiation field simulation. *Photochem. Photobiol.* ???, ???–???. (In press) **7**
16. Frenkel, D. (2004) Introduction to Monte Carlo methods. In *Computational Soft Matter: From Synthetic Polymers to Proteins, Lecture Notes* (Edited by N. Attig, K. Binder, H. Grubmüller and K. Kremer), pp. 29–60. John von Neumann Institute for Computing, Jülich.
17. Imoberdorf, G. E., O. M. Alfano, A. E. Cassano and H. A. Irazoqui (2007) Monte Carlo model of UV-radiation interaction with TiO₂-coated spheres. *AIChE J.* **53**, 2688–2703.
18. Atlas, R. M. (2005) *Handbook of Media for Environmental Microbiology*, pp. ???–???. Taylor & Francis, Boca Raton. **8**
19. Clesceri, L. S., A. E. Greenberg and A. D. Eaton (1999) *Standard Methods for the Examination of Water and Wastewater*, 20th edn, pp. ???–???. American Public Health Association, Washington, DC.
20. Ritchie, R. J. (2008) Universal chlorophyll equations for estimating chlorophylls *a*, *b*, *c*, and *d* and total chlorophylls in natural assemblages of photosynthetic organisms using acetone, methanol, or ethanol solvents. *Photosynthetica* **46**(1), 115–126.
21. Brucato, A. and L. Rizzuti (1997) Simplified modeling of radiant fields in heterologous photoreactors. I. Case of zero reflectance. *Ind. Eng. Chem. Res.* **36**, 4740–4747.
22. Evers, E. G. (1991) A model for light-limited continuous cultures: growth, shading, and maintenance. *Biotechnol. Bioeng.* **38**, 254–259.
23. Katsuda, T., T. Arimoto, K. Igarashi, M. Azuma, J. Kato, S. Takakuwa and H. Ooshima (2000) Light intensity distribution in the external illuminated cylindrical photo-bioreactor and its application to hydrogen production by *Rhodobacter capsulatus*. *Biochem. Eng. J.* **5**, 157–164.
24. Kurata, H. and S. Furusaki (1993) Nonisotropic scattering model for estimation of light absorption rates in a suspension culture of *Coffea arabica* cells. *Biotechnol. Prog.* **9**, 86–92.
25. Pilon, L., H. Berberoglu and R. Kandilian (2011) Radiation transfer in photobiological carbon dioxide fixation and fuel production by microalgae. *J. Quant. Spectrosc. Ra.* **112**(17), 2639–2660.
26. Berberoglu, H. and L. Pilon (2009) Radiation characteristics of *Botryococcus braunii*, *Chlorococcum littorale*, and *Chlorella* sp. used for CO₂ fixation and biofuel production. *J. Quant. Spectrosc. Ra.* **110**, 1879–1893.
27. Berberoglu, H., A. Melis and L. Pilon (2008) Radiation characteristics of *Chlamydomonas reinhardtii* CC125 and its truncated chlorophyll antenna transformants *tla1*, and *tla1-CWp*. *Int. J. Hydrogen Energy* **33**(22), 6467–6483.
28. Csögör, Z., M. Herrenbauer, K. Schmidt and C. Posten (2001) Light distribution in a novel photobioreactor—modelling for optimization. *J. Appl. Phycol.* **13**, 325–333.
29. Rosello Sastre, R., Z. Csögör, I. Perner-Nochta, P. Fleck-Schneider and C. Posten (2007) Scale-down of microalgae cultivations in tubular photo-bioreactors—a conceptual approach. *J. Biotechnol.* **132**, 127–133.

Graphical Abstract

The contents of this page will be used as part of the graphical abstract of html only. It will not be published as part of main article.



A Monte Carlo simulation program is developed and used as a predictive autonomous program applied to the modeling of experiments that reproduce the common illumination conditions found in processes of large scale production of microalgae. It can be applied to assess as to what extent the scattering phenomena are important for the prediction of the radiant energy density and to compute this property inside photobioreactors with the goal to optimize its design and their operating conditions. The module is validated by comparing the results of experimental measurements made on algal suspensions with those predicted by the Monte Carlo program.

Author Query Form

Journal: PHP

Article: 1149

Dear Author,



During the copy-editing of your paper, the following queries arose. Please respond to these by marking up your proofs with the necessary changes/additions. Please write your answers on the query sheet if there is insufficient space on the page proofs. Please write clearly and follow the conventions shown on the attached corrections sheet. If returning the proof by fax do not write too close to the paper's edge. Please remember that illegible mark-ups may delay publication.

Many thanks for your assistance.

Query reference	Query	Remarks
1	AUTHOR: Please confirm that graphical abstract is fine for online publication.	
2	AUTHOR: This article has been lightly edited for grammar, style and usage. Please compare it with your original document and make changes on these pages. Please limit your corrections to substantive changes that affect meaning. If no change is required in response to a question, please write "OK as set" in the margin. Copy editor	
3	AUTHOR: Table 1 was not cited in the text. An attempt has been made to insert the table into a relevant point in the text—please check that this is OK. If not, please provide clear guidance on where it should be cited in the text.	
4	AUTHOR: Please check all the equations to ensure that they have been entered correctly.	
5	AUTHOR: Figure 2 was not cited in the text. An attempt has been made to insert the figure into a relevant point in the text—please check that this is OK. If not, please provide clear guidance on where it should be cited in the text.	
6	AUTHOR: Please provide the page range for reference [1].	
7	WILEY-BLACKWELL: Please update the volume number and page range/doi number for reference [15].	
8	WILEY-BLACKWELL: Please update the page range for references [18] & [19].	
9	AUTHOR: In Fig. 5(a), symbol (○, open circle) has not been mentioned in the physical figure. Please check.	

Proof Correction Marks

Please correct and return your proofs using the proof correction marks below. For a more detailed look at using these marks please reference the most recent edition of The Chicago Manual of Style and visit them on the Web at: <http://www.chicagomanualofstyle.org/home.html>

<i>Instruction to typesetter</i>	<i>Textual mark</i>	<i>Marginal mark</i>
Leave unchanged	... under matter to remain	<i>stet</i>
Insert in text the matter indicated in the margin	^	^ followed by new matter
Delete	Ʒ through single character, rule or underline or Ʒ through all characters to be deleted	<i>del</i>
Substitute character or substitute part of one or more word(s)	ƶ through letter or — through characters	new character ƶ or new characters ƶ
Change to italics	— under matter to be changed	<i>ital</i>
Change to capitals	≡ under matter to be changed	<i>Caps</i>
Change to small capitals	≡ under matter to be changed	<i>sc</i>
Change to bold type	~ under matter to be changed	<i>bf</i>
Change to bold italic	~ under matter to be changed	<i>bf+ital</i>
Change to lower case	Ɔ	<i>lc</i>
Insert superscript	√	√ under character e.g. √
Insert subscript	^	^ over character e.g. ^
Insert full stop	⊙	⊙
Insert comma	↵	↵
Insert single quotation marks	↵ ↵	↵ ↵
Insert double quotation marks	↵ ↵	↵ ↵
Insert hyphen	=	=
Start new paragraph	¶	¶
Transpose	┌┐	┌┐
Close up	linking  characters	
Insert or substitute space between characters or words	#	#
Reduce space between characters or words	˘	˘